Hypersingular Integral-Equation Method for Wave Diffraction about Arbitrary, Shell-Like Vertical Cylinders in Finite-Depth Waters

By Mohamed Hariri Nokob and Ronald W. Yeung*
University of California at Berkeley
Berkeley, CA 94720-1740, USA,
Correspondence author: E-mail: rwyeung@berkeley.edu

Highlights:

- A hypersingular integral-equation method is used to obtain the wave-exciting loads on and free-surface elevations around a bottom-mounted, arbitrarily shaped thin vertical cylinder.
- The effects of an opening in the cylindrical shell are discussed.

1. Introduction

We present a method to solve for the wave-diffraction loads on thin or shell-like bottom-mounted vertical cylinders of arbitrary cross-sections in an inviscid wavy field. Solutions for the flow about solid cylinders are well treated, e.g., [1][2]. However, the treatment is not as straight-forward when the cylinder is a thin shell and of arbitrary shape. The conventional boundary-integral formulation will lead to a hypersingular integral equation, with more precaution in the evaluation of the kernel. The hypersingular integral method was successfully employed in [3] for a flapping plate. The procedure used in that work and others (e.g. see [4][5]) is modified according to our recent work [6] to achieve a simpler form. For demonstration, the method is used to solve for the wave field about an elliptical cylindrical shell with an opening. The effects of the opening location and its size on the diffraction pattern and forces are discussed.

2. Problem Formulation

Consider the dimensionless total potential Φ^S:

$$\Phi^S(x,y,z,t) = \mathrm{Re}\{\phi^S(x,y,z)e^{-i\omega t}\}, \qquad \phi^S = \phi^0 + \phi, \tag{1}$$

being harmonic in time with an angular frequency ω. Here, ϕ^0 is the known incident-wave potential and ϕ is the unknown diffracted one. We use the normalization $\phi = \bar{\phi}/\eta_0\sqrt{ga}$ for all potentials in this work. The overbar denotes dimensional potentials, a is a characteristic length of the body, g the constant of gravity and η_0 the incident-wave amplitude. Hereafter, all length variables and wave numbers are normalized using a. The domain is considered laterally unbounded and the water depth is given by h. Consider a coordinate system on the calm-water free surface with the y axis pointing upwards (Fig. 1). The governing equations for the unknown ϕ are:

$$\nabla^2\phi = 0, \tag{2}$$

$$\frac{\partial\phi}{\partial y} - \nu\phi = 0, \quad \nu = \frac{\omega^2 a}{g}, \quad y = 0, \tag{3}$$

$$\frac{\partial\phi}{\partial y} = 0, \quad y = -h, \tag{4}$$

$$\frac{\partial\phi}{\partial n} = -\frac{\partial\phi^0}{\partial n}, \quad P \in B \tag{5}$$

as well as a radiation condition in the farfield. Here $P(x,y,z)$ is the field point and B is the shell surface with a normal vector $\vec{n}$ pointing out of the body. We then write:

$$\phi(x,y,z) = \varphi(x,z)Y(y), \tag{6}$$

$$Y(y) = \frac{\cosh(\kappa(y+h))}{M}, \quad \text{with } M = \sqrt{\frac{\sinh(2\kappa h)}{4\kappa} + \frac{h}{2}}. \tag{7}$$

where φ is an unknown potential in the horizontal plane and κ is the wave number of the incident wave that satisfies the usual dispersion relation: $\kappa\tanh(\kappa h) = \nu$. Y satisfies (3) and (4). ϕ^0 can be also decomposed in the same manner:

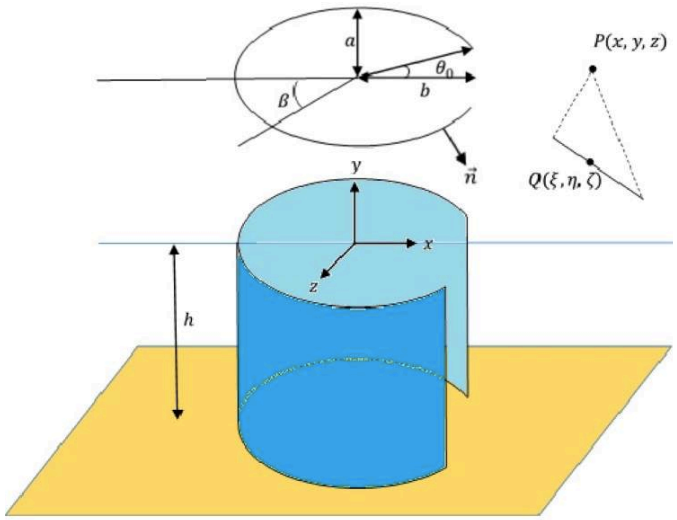

Fig. 1: The elliptical cylindrical shell considered and coordinate system

$$\phi^0(x,y,z) = \varphi^0(x,z)Y(y),$$

$$\varphi^0 = \frac{e^{i\kappa(x\cos\beta + z\sin\beta)}}{i\sqrt{\nu}Y(0)}.$$

Here, β denotes the incident wave direction (Fig. 1). The governing equations for the unknown "modal potential" thus become:

$$\nabla^2\varphi + \kappa^2\varphi = 0, \tag{8}$$

$$\frac{\partial\varphi}{\partial n} = -\frac{\partial\varphi^0}{\partial n}. \tag{9}$$

Equations (8)-(9) will be solved using a boundary integral method by representing φ as a normal dipole sheet (see [7]) and by applying (9). Thus,

$$\frac{\partial\varphi}{\partial n_P} = \int_C [\varphi]\frac{\partial^2 G}{\partial n_P \partial n_Q} ds. \tag{10}$$

The brackets symbolize the potential jump across the body while $P(x,z)$, $Q(\xi,\varsigma)$ represent collocation and integration points in the usual manner, respectively. The integration is taken over only one side of the body contour. The fundamental solution G satisfies the radiation condition and is given by [8]:

$$G = -\frac{i}{4}H_0(\kappa R), \tag{11}$$

$$R = |PQ| = \sqrt{(x-\xi)^2 + (z-\varsigma)^2}.$$

with H_0 being the Hankel function of the first kind and $n_P = [\sin\alpha, -\cos\alpha]$, $n_Q = [\sin\theta, -\cos\theta]$, where α,θ are the slope angles of the body curve (see Fig. 1). Thus,

$$\frac{\partial^2 G}{\partial n_P \partial n_Q} = \frac{i\kappa_n}{4R^2}\left(\frac{2H_1(\kappa_n R)}{R} - \kappa_n H_0(\kappa_n R)\right)\times \begin{pmatrix}(\xi-x)^2\sin\alpha\sin\theta + (\varsigma-z)^2\cos\alpha\cos\theta \\ -(\xi-x)(\varsigma-z)\sin(\theta+\alpha)\end{pmatrix} - \frac{i\kappa_n}{4R}H_1(\kappa_n R)\cos(\theta-\alpha). \tag{12}$$

3. Numerical Treatment

To solve the problem, the body shape is divided into N flat panels $C_j[(\xi_j,\varsigma_j),(\xi_{j+1},\varsigma_{j+1})]$ where we assume a constant potential jump across each of these panels. We also introduce an integration parameter $t \in [0,1]$ over each C_j so that

$$\int_{C_j}\frac{\partial^2 G}{\partial n_P \partial n_Q} ds = \frac{ds}{dt}\int_{C_j}\frac{\partial^2 G}{\partial n_P \partial n_Q} dt, \tag{13}$$

$$\begin{aligned}\xi &= (\xi_{j+1} - \xi_j)t + \xi_j, \\ \varsigma &= (\varsigma_{j+1} - \varsigma_j)t + \varsigma_j, \\ s &= S_j t.\end{aligned} \tag{14}$$

Here S_j is the panel length. The integration in (13) is standard except when Q approaches P. In that case, a Taylor expansion of the integrand around the point $t = t_s$ where the troublesome singularity occurs leads to

$$\frac{\partial^2 G}{\partial n_P \partial n_Q} = \frac{\kappa^2}{4\pi S_j^2}\left(\frac{4}{\kappa^2 S_j^2 (t-t_s)^2} + 1\right)\times \begin{pmatrix}(\xi_{j+1}-\xi_j)^2\sin\alpha\sin\theta + (\varsigma_{j+1}-\varsigma_j)^2\cos\alpha\cos\theta \\ -(\xi_{j+1}-\xi_j)(\varsigma_{j+1}-\varsigma_j)\sin(\theta+\alpha)\end{pmatrix} - \frac{i\kappa^2}{8}\left(1 + \frac{2i}{\pi}\left(\ln\frac{\kappa S_j|t-t_s|}{2} + \gamma - \frac{2}{\kappa^2 S_j^2 (t-t_s)^2} - \frac{1}{2}\right)\right)\times \cos(\theta-\alpha) + O(R^2\ln R). \tag{15}$$

Equations (14), along with the fact that $R = S|t - t_s|$ were used in getting (15). Clearly, a hypersingular point of order R^{-2} exists. This equation can be integrated analytically between two points $0 \le t_1 \le t_s \le t_2 \le 1$ on a straight-line panel on B:

$$\int_{t_1}^{t_2}\frac{\partial^2 G}{\partial n_P \partial n_Q} dt = \frac{\kappa^2\Delta t}{4\pi S_j^2}\left(1 - \frac{4}{\kappa^2 S_j^2 \Delta t_1 \Delta t_2}\right)\times \begin{pmatrix}(\xi_{j+1}-\xi_j)^2\sin\alpha\sin\theta + (\varsigma_{j+1}-\varsigma_j)^2\cos\alpha\cos\theta \\ -(\xi_{j+1}-\xi_j)(\varsigma_{j+1}-\varsigma_j)\sin(\theta+\alpha)\end{pmatrix} - \frac{i\kappa^2\Delta t\cos(\theta-\alpha)}{8}\left(1 + \frac{2i}{\pi}\begin{pmatrix}\frac{\Delta t_2}{\Delta t}\ln\frac{\kappa S_j \Delta t_2}{2} + \\ \frac{\Delta t_1}{\Delta t}\ln\frac{\kappa S_j \Delta t_1}{2} + \\ \gamma + \frac{2}{\kappa^2 S_j^2 \Delta t_1 \Delta t_2} - \frac{3}{2}\end{pmatrix}\right). \tag{16}$$

Here, we defined $(\Delta t = t_2 - t_1, \Delta t_2 = t_2 - t_s, \Delta t_1 = t_s - t_1)$. After discretization of the contour and collocation, a system of equations is obtained and the solution is the potential jumps across the different panels. The source vector of the system is obtained from (9) after being applied at the collocation points of choice. The midpoints of the panels are chosen in this work.

4. Wave Loads and Wave Field

The loads on the body can be obtained by integrating the dynamic pressure over the surface. We define the excitation load in dimensionless form as $f_j = \bar{F}_j / \rho\eta_0 g a^m$. Here ρ is the fluid density and the exponent m is 2 for forces and 3 for moments. The loads are then given by:

$$\begin{aligned} f_j &= i\sqrt{\nu}\int_C\int_{-h}^{0}[\phi]\,Y(y)n_j dy ds \\ &= i\sqrt{\nu}\sum_{q=1}^{N}[\phi]_q\int_{-h}^{0} Y n_j dy S_q. \end{aligned} \tag{17}$$

$$n_j = \begin{cases} n_x, n_z, & j = 1,2 \\ (y+h).(n_x, n_z), & j = 4,5, \\ z n_x - x n_z, & j = 6, \end{cases} \tag{18}$$

In (17), q is the circumferential index of the straight-line elements. The moments for *j=4, 5* are taken about *z* and *x* axes, respectively, but over the ocean floor *(y=-h)*. The last moment is about the y-axis. Note that the incident wave does not contribute to the loads on the body because of the zero thickness property. We are also interested in the free surface elevation which can be obtained from the integral equation as:

$$\frac{\eta^D}{\eta_0} = e^{i\kappa(x\cos\beta + z\sin\beta)} + i\sqrt{\nu}Y(0)\int_C [\varphi]\frac{\partial G}{\partial n_Q}ds \tag{19}$$

$$= e^{i\kappa(x\cos\beta + z\sin\beta)} + i\sqrt{\nu}Y(0)\sum_{q=1}^{N}[\varphi]_q\int_{C_q}\frac{\partial G}{\partial n_Q}ds,$$

$$\frac{\partial G}{\partial n_Q} = \frac{i\kappa}{4}\frac{H_1(\kappa R)}{R}\left\{(\xi - x)n_\xi + (\varsigma - z)n_\varsigma\right\}. \tag{20}$$

The integrals in (19) can be handled by standard quadrature.

5. Results and Discussions

The procedure was verified by comparing the results for a closed circular cylinder to those in the literature [9]. In this paper, we will present just results for an elliptical cylinder with major and minor axes $b = 1.5, a = 1$, respectively (Fig. 1). 100 panels were found adequate to achieve a relative error less than 1%. We first present the free surface elevation results for total wave field over the elliptic shell in head and beam waves (Fig. 2 and 3).

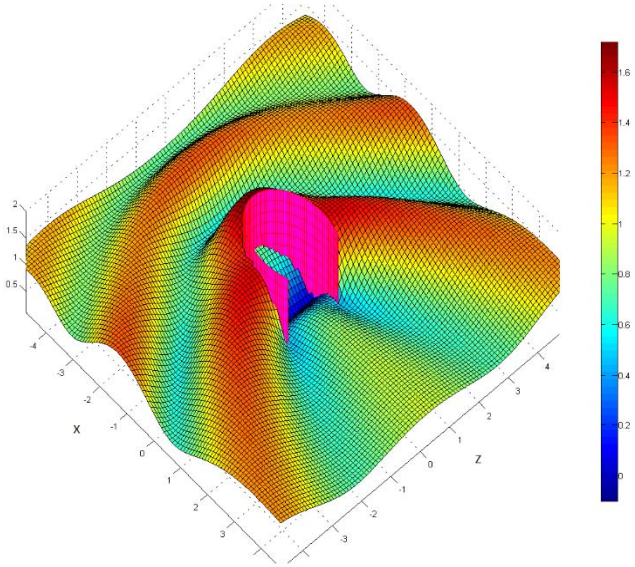

Fig. 2: Free-surface elevation around an elliptic shell with opening $\theta_0 = \pi/3$ for a wave incident at a direction $\beta = 0$ and $\kappa = 1.5$

The results for the head wave (Fig. 2) indicate how the cylinder effectively shields the area downstream from the wave effects. Particularly of interest is the area inside the shell where no wave effects are observed at all. The beam wave results (Fig. 3) show an asymmetry in the shape of the field downstream of the body because of the presence of the opening. Effectively, a calm region spreads downstream from the edge of the shell. Higher waves are observed inside, though when compared to the previous case.

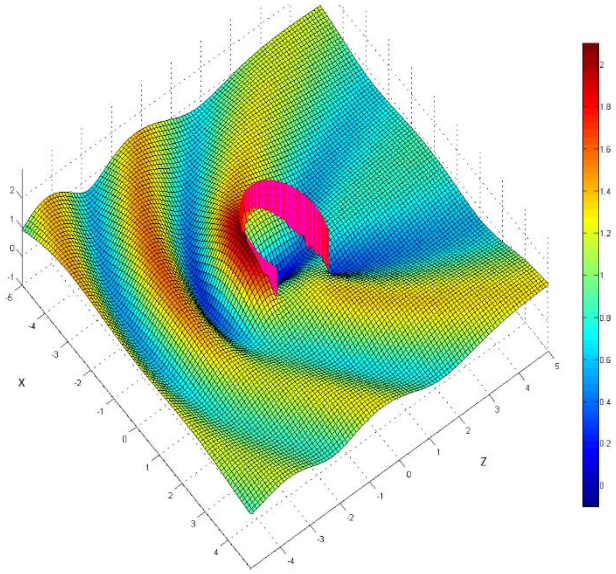

Fig. 3: Free surface elevation around an elliptic shell with opening $\theta_0 = \pi/3$ for a wave incident at a direction $\beta = \pi/2$ and $\kappa = 1.5$

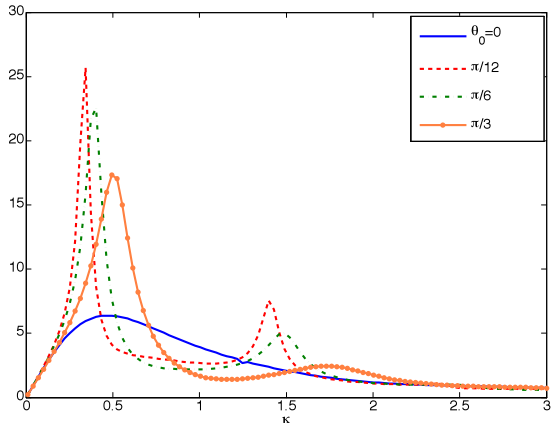

Fig. 4: Force f_1 due to a wave incident at $\beta = 0$

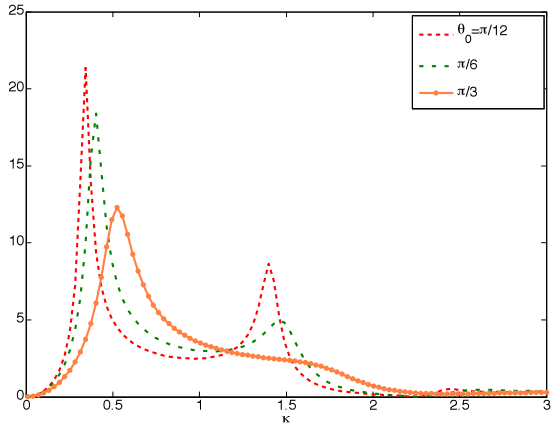

Fig. 5: Force f_1 due to a wave incident at $\beta = \pi/2$

Results for the loads on the body due to incident waves of different frequencies are plotted in (Figs. 4-7) against the wavenumber. The results in (Fig. 4) show that the forces on the body in the *x*-direction significantly increase at frequencies

where the closed body attains its peak forces. This however decreases with the increased opening size.

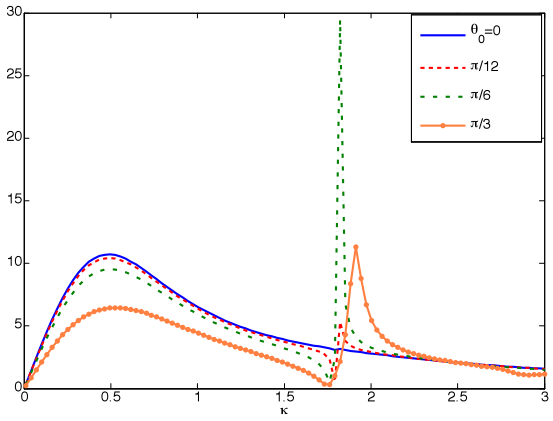

Fig. 6: Force f_2 due to a wave incident at $\beta = \pi/2$

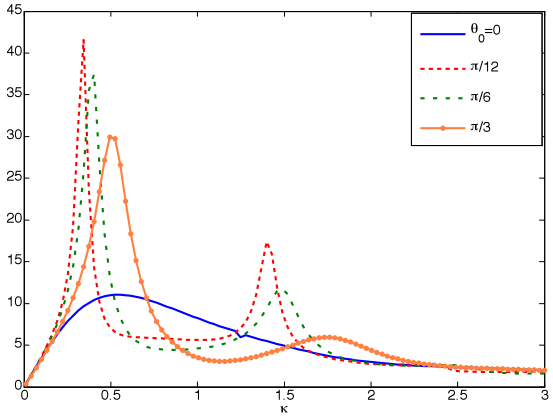

Fig. 7: Pitching Moment f_4 due to a wave incident at $\beta = 0$

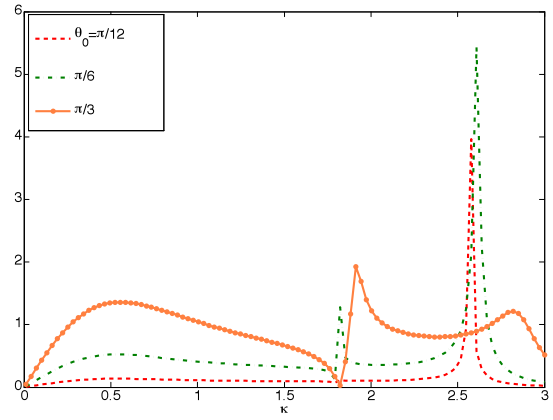

Fig. 8: Yawing torque f_6 due to a wave incident at $\beta = \pi/2$

An increase in wave frequency of the incident wave leads to smaller forces on the open body to increase again at high frequencies. This can be attributed to the interaction of waves inside the body (the opening effect) being superposed over the body effect present when the body is closed. For beam incident waves, the force along the x-axis is nonzero when the body is opened (Fig. 5). In general, two peaks are observed in the figures for open bodies. The first peak is present for the closed body as well and can be attributed to the body shape and size. This peak is enhanced as the body is opened because of interference effects as already explained. The second peak emerges entirely because of the opening but is lower than the first peak. This peak is also observed at these frequencies for radiation forces when the body is made to move. It is therefore attributed to the resonance of the internal region of the shell.

In general, the open body with the smallest opening is suffering the highest loads. Interestingly enough, the loads in the wave direction for beam waves decrease as the body is opened contrary to the results in head seas. The second peak is still observed though.

The results for the moments are similar to those for the corresponding forces. We include one case in (Fig. 7) which shows the wave moment about an axis passing through the cylinder bottom and parallel to the z-axis. The similarity to the results in (Fig. 4) is obvious. This is to be expected as this moment results from forces in the x-direction applied about the prescribed axis.

The final figure (Fig. 8) shows the torque on the body in a beam wave field. This torque is non-existent for head waves even when the body is opened because of symmetry. It only appears for an open body in beam waves. Three different peaks are observed for this load with spikier ones at higher frequencies, where this load seems to be more important. Forces in both the *x* and *z* directions contribute to this torque which might explain its more complex behavior.

In the Workshop, new results [10] for the radiation problems will be presented as well.

6. References

[1] R. C. MacCamy and R. A. Fuchs, "Wave Force on Piles: A Diffraction Theory," U.S. Army Coastal Engineering Research Center), Technical Memorandum 69, 1954.

[2] H. S. Chen and C. C. Mei, "Wave forces on a stationary platform of elliptical shape," *J. Ship Res.*, 1973.

[3] E. Renzi and F. Dias, "Resonant behavior of an oscillating wave energy converter in a channel," *J. Fluid Mech.*, vol. 701, pp. 482–510, 2012.

[4] N. F. Parsons and P. A. Martin, "Scattering of water waves by submerged plates using hypersingular integral equations,"*Appl. Ocean. Res.*, vol. 14, pp. 313–321, 1992.

[5] L. Farina and P. A. Martin, "Scattering of water waves by a submerged disc using a hypersingular integral equation," *Appl. Ocean. Res.*, vol. 20, pp. 121–134, 1998.

[6] R. W. Yeung and M. Hariri Nokob, "Hypersingular integral-equation solution for a finite-draft surface-piercing cylindrical shell at high- and low-frequency," in *The 28th IWWWFB*, L'Isle sur la Sorgue, France, 2013.

[7] R. W. Yeung, "Numerical Methods in Free-Surface Flows," *Annual Review of Fluid Mechanics*, vol. 14, no. 1, pp. 395–442, 1982.

[8] A. J. Burton and G. F. Miller, "The application of integral equation methods to the numerical solution of some exterior boundary-value problems," *Prco. Roy. Soc. London. A,* vol. 323, pp. 201–210, Jun. 1971.

[9] C. J. R. Garrett, "Wave forces on a circular dock," *J. Fluid Mech.*, vol. 46, pp. 129–139, 1971.

[10] M. Hariri Nokob and R. W. Yeung, "Computation of arbitrary thin-shell vertical cylinders in a wave field by a hypersingular integral-equation method," in *Proc. 33rd OMAE Conference*, San Francisco, 2014.